A&A 649, A76 (2021)
https://doi.org/10.1051/0004-6361/202140360

Astronomy & Astrophysics

Broadband X-ray spectra and timing of the accreting millisecond pulsar Swift J1756.9–2508 during its 2018 and 2019 outbursts

Z. S. Li[1], L. Kuiper[2], M. Falanga[3], J. Poutanen[4,5,6], S. S. Tsygankov[4,5], D. K. Galloway[7,8], E. Bozzo[9], Y. Y. Pan[1], Y. Huang[10], S. N. Zhang[10], and S. Zhang[10]

[1] Key Laboratory of Stars and Interstellar Medium, Xiangtan University, Xiangtan 411105, Hunan, PR China
e-mail: lizhaosheng@xtu.edu.cn
[2] SRON-Netherlands Institute for Space Research, Sorbonnelaan 2, 3584 CA Utrecht, The Netherlands
[3] International Space Science Institute (ISSI), Hallerstrasse 6, 3012 Bern, Switzerland
[4] Department of Physics and Astronomy, 20014 University of Turku, Finland
[5] Space Research Institute of the Russian Academy of Sciences, Profsoyuznaya str. 84/32, 117997 Moscow, Russia
[6] Nordita, KTH Royal Institute of Technology and Stockholm University, Roslagstullsbacken 23, 10691 Stockholm, Sweden
[7] School of Physics and Astronomy, Monash University, Melbourne, VIC 3800, Australia
[8] OzGRav-Monash, School of Physics and Astronomy, Monash University, Clayton, VIC 3800, Australia
[9] University of Geneva, Department of Astronomy, Chemin d'Ecogia 16, 1290 Versoix, Switzerland
[10] Key Laboratory of Particle Astrophysics, Institute of High Energy Physics, Chinese Academy of Sciences, 19B Yuquan Road, Beijing 100049, PR China

Received 15 January 2021 / Accepted 26 February 2021

ABSTRACT

The accreting millisecond X-ray pulsar Swift J1756.9–2508 launched into an outburst in April 2018 and June 2019 – 8.7 years after the previous period of activity. We investigated the temporal, timing, and spectral properties of these two outbursts using data from NICER, *XMM-Newton*, *NuSTAR*, INTEGRAL, *Swift*, and *Insight*-HXMT. The two outbursts exhibited similar broadband spectra and X-ray pulse profiles. For the first time, we report the detection of the pulsed emission up to ∼100 keV that was observed by *Insight*-HXMT during the 2018 outburst. We also found the pulsation up to ∼60 keV that was observed by NICER and *NuSTAR* during the 2019 outburst. We performed a coherent timing analysis combining the data from the two outbursts. The binary system is well described by a constant orbital period over a time span of ∼12 years. The time-averaged broadband spectra are well fitted by the absorbed thermal Comptonization model COMPPS in a slab geometry with an electron temperature, kT_e = 40–50 keV, Thomson optical depth $\tau \sim 1.3$, blackbody seed photon temperature $kT_{bb,seed} \sim 0.7$–0.8 keV, and hydrogen column density of $N_H \sim 4.2 \times 10^{22}$ cm^{-2}. We searched the available data for type-I (thermonuclear) X-ray bursts, but found none, which is unsurprising given the estimated low peak accretion rate (≈0.05 of the Eddington rate) and generally low expected burst rates for hydrogen-poor fuel. Based on the history of four outbursts to date, we estimate the long-term average accretion rate at roughly $5 \times 10^{-12}\,M_\odot\,\mathrm{yr}^{-1}$ for an assumed distance of 8 kpc. The expected mass transfer rate driven by gravitational radiation in the binary implies the source may be no closer than 4 kpc. Swift J1756.9–2508 is the third low mass X-ray binary exhibiting "double" outbursts, which are separated by much shorter intervals than what we typically see and are likely to result from interruption of the accretion flow from the disk onto the neutron star. Such behavior may have important implications for the disk instability model.

Key words. stars: neutron – X-rays: general – pulsars: individual: Swift J1756.9–2508 – radiation mechanisms: non-thermal – X-rays: binaries

1. Introduction

Swift J1756.9–2508 was discovered by *Swift*-BAT during its 2007 outburst (Krimm et al. 2007a; Linares et al. 2008). Coherent X-ray pulsations at a frequency of ∼182 Hz confirmed the compact object to be an accreting millisecond X-ray pulsar (AMXP) (Markwardt et al. 2007). In the following observations, carried out by *Swift* and RXTE, an orbital period of 54.7 min was measured and, based on its mass function, the mass of the companion star – a highly evolved white dwarf – was determined to be in the range of 0.0067−0.03 $M_\odot$ (Krimm et al. 2007b).

The AMXPs are rapidly spinning, old, recycled neutron stars (NSs) hosted in low-mass X-ray binaries (LMXB). As a binary system evolves through phases of accretion onto the NS, it gains angular momentum from the accreted material, which is sufficient to spin-up the NS to a rotation period equilibrium in the millisecond range, that is, the recycling of old radio-pulsars to millisecond periods (Alpar et al. 1982; Wijnands & van der Klis 1998; Falanga et al. 2005b; Papitto et al. 2013). On the other hand, between the outbursts, long-term monitoring shows some AMXPs to exhibit spin-down in quiescence (see, e.g., Hartman et al. 2009; Patruno et al. 2010; Papitto et al. 2010). For reviews of the properties of these objects, we refer to Wijnands (2003), Poutanen (2006), Patruno & Watts (2021), Campana & Di Salvo (2018), Papitto et al. (2020), and Di Salvo & Sanna (2020).

The source, Swift J1756.9–2508, was shown to have undergone another three outbursts: in 2009 (Patruno et al. 2009a), 2018 (Sanna et al. 2018c; Bult et al. 2018a; Rai & Paul 2019; Chakraborty & Bhattacharyya 2018), and 2019 (Sanna et al. 2019). For the first three recurrent outbursts between 2007 and 2018, there was no orbital period variation detected (Krimm et al. 2007b; Patruno et al. 2010; Bult et al. 2018a; Sanna et al. 2018c). Moreover, the upper limit on the orbital period derivative is $|\dot{P}_{orb}| < 7.4 \times 10^{-13}$ s s^{-1} from the total 11-year span of the observations, which is consistent with the prediction of a conservative mass transfer in the binary system (Bult et al. 2018a).

Swift J1756.9–2508 exhibited long-term spin-down behavior with a spin frequency derivative of $|\dot{\nu}| \lesssim 3 \times 10^{-13}$ Hz s^{-1}, measured by Patruno et al. (2010), $|\dot{\nu}| \sim 7.3 \times 10^{-16}$ Hz s^{-1} by Bult et al. (2018a) and a smaller value $|\dot{\nu}| \sim 4.8 \times 10^{-16}$ Hz s^{-1} by Sanna et al. (2018c). Assuming that the rotational energy loss due to the magnetic dipole emission dominated the spin evolution of Swift J1756.9–2508, the magnetic field strength at the stellar magnetic poles was constrained to the range of $(3-6) \times 10^8$ G (see, e.g., Patruno et al. 2010; Bult et al. 2018a; Sanna et al. 2018c, and references therein).

Most NSs hosted in LMXB systems exhibit type I X-ray bursts (Galloway et al. 2020). Type I bursts are thermonuclear explosions on the surface of the accreting NS, triggered by unstable hydrogen or helium burning. They are typically characterized by a fast rise time of ∼1−2 s, followed by exponential-like decays, as well a gradual softening due to the cooling of the NS photosphere, with durations ranging from seconds to minutes and recurrence times from a few hours to days (see, e.g., Lewin et al. 1993; Strohmayer & Bildsten 2006; Galloway & Keek 2021, for reviews). The burst spectra are described by a blackbody with peak temperatures reaching $kT_{\rm bb} \approx 3$ keV, where the luminosity can reach the Eddington limit, $L_{\rm Edd} \approx 2 \times 10^{38}$ erg s^{-1}, and the total burst energy release is on the order of $\sim 10^{39}$ erg (see Lewin et al. 1993; Strohmayer & Bildsten 2006; Galloway et al. 2008, for a review). Several thousand bursts have been observed to date (see, e.g., Galloway et al. 2008, 2020). However, 7 sources (including Swift J1756.9–2508) out of 21 known AMXPs, including 20 AMXPs mentioned in Table 1 from Di Salvo & Sanna (2020) as well as the newly confirmed AMXP IGR J17494−3030 (Ng et al. 2021), have not shown type-I X-ray bursts during their outbursts. Hence, the distance to Swift J1756.9–2508 is still unknown. Below, for a number of estimates, we assume a distance of 8 kpc (since the source lies close to the direction to the Galactic center).

In this paper, we report on the broadband (1–300 keV) spectral and timing results using the available high-energy data, including INTEGRAL (20−300 keV), two *NuSTAR* (3−79 keV), one *XMM-Newton* (1−10 keV), eight NICER (0.2−12 keV), nine *Swift*, and five *Insight*-HXMT (5−250 keV) observations during the 2018 outburst from Swift J1756.9–2508, as well as one *NuSTAR*, one *Swift*, and seven NICER observations during its 2019 outburst. All the monitoring observations have been applied to shed light on the physical processes acting upon Swift J1756.9–2508.

2. Observations and data reduction

We reduce the data from Swift J1756.9–2508 collected during its 2018 and 2019 outbursts. For the 2018 outburst, INTEGRAL was the first to detect the enhanced X-ray emission from Swift J1756.9–2508 (Mereminskiy et al. 2018). Several high-energy facilities carried out the follow-up obse rvations covering the whole outburst (Bult et al. 2018b,c; Krimm et al. 2018; Mazzola et al. 2018; Kuiper et al. 2018). During the 2019 outburst, NICER, *NuSTAR*, and *Swift* observed Swift J1756.9–2508 (Sanna et al. 2019). Below, we introduce the data reduction part for all instruments. In addition, we provide in Table 1 a log of all observations during the 2018 and 2019 outbursts. We adopted Solar System ephemeris DE405 and the X-ray position of Swift J1756.9–2508 (Krimm et al. 2007b) to apply the barycentering corrections for the timing analysis using INTEGRAL (Sect. 2.1), NICER (Sect. 2.2), *NuSTAR* (Sect. 2.3), *XMM-Newton* (Sect. 2.4), and *Insight*-HXMT (Sect. 2.5) observations.

Table 1. Observations of Swift J1756.9–2508 for the 2018 and 2019 outbursts, respectively.

Mission	Obs. ID	Instrument	Date [a] (d)	Exposure (ks)
2018 outburst				
NuSTAR	90402313002	FPMA/FPMB	8.36	39.5
	90402313004	FPMA/FPMB	14.13	61.0
NICER	1050230101	XTI	3.64	7.5
	1050230102	XTI	4.61	7.1
	1050230103	XTI	7.89	2.4
	1050230104	XTI	8.02	10.7
	1050230105	XTI	9.33	4.1
	1050230106	XTI	10.02	6.2
	1050230107	XTI	11.06	5.0
	1050230108	XTI	25.85	1.5
XMM-Newton	0830190401	RGS/MOS/PN	8.09	66
INTEGRAL	1936, 1937	ISGRI	−1.23, 1.42	129
	1939 (ToO)	ISGRI	7.68	85
	1940	ISGRI	10.01	
	1942	ISGRI	14.91	190 [b]
	1944	ISGRI	20.20	
Insight-HXMT	P011469200101	ME & HE	5.13	4.3
	P011469200102	ME & HE	5.33	1.1
	P011469200103	ME & HE	5.47	0.3
	P011469200104	ME & HE	5.60	1.2
	P011469200105	ME & HE	5.71	5.9
Swift	00030952018	XRT	2.67	1.0
	00088662001	XRT	8.77	2.2
	00030952019	XRT	9.78	1.0
	00030952020	XRT	10.38	0.4
	00030952021	XRT	12.59	1.3
	00088662002	XRT	14.82	2.1
	00030952022	XRT	18.75	1.0
	00030952023	XRT	24.59	1.2
	00030952024	XRT	27.44	1.4
2019 outburst				
NuSTAR	90501329001	FPMA/FPMB	11.85	37.7
NICER	2050230101	XTI	9.10	1.5
	2050230102	XTI	9.56	3.6
	2050230103	XTI	11.10	5.4
	2050230104	XTI	11.50	11.7
	2050230105	XTI	16.51	1.1
	2050230106	XTI	19.02	1.7
	2050230107	XTI	21.16	1.1
Swift	00030952025	XRT	10.53	0.9

Notes. [a]The start time of the observations since MJD 58208 and 58644.5 for the 2018 and 2019 outbursts, respectively. [b]The total exposure time of Rev. 1940, 1942, and 1944.

2.1. INTEGRAL

Our INTEGRAL (Winkler et al. 2003) data set comprises all the observations covering the 2018 outburst. It consists of 160 stable pointings (science windows, ScWs) with a source position offset from the center of the field of view $\lesssim 12\overset{\circ}{.}0$. The different satellite pointings in the direction of Swift J1756.9–2508, each lasting ∼2−3 ks, were performed between March 29 and April 20, 2018. Specifically, the satellite revolutions included in the analysis were: 1936–1937, 1939–1940, 1942, and 1944. This includes also a dedicated Target of Opportunity (ToO) observation during revolution 1939 beginning on April 7 (MJD 58215.81170). The data reduction was performed using the standard Offline Science Analysis (OSA[1]) version 10.2, distributed by the Integral Science Data Center (Courvoisier et al. 2003).

[1] http://www.isdc.unige.ch/integral/analysis

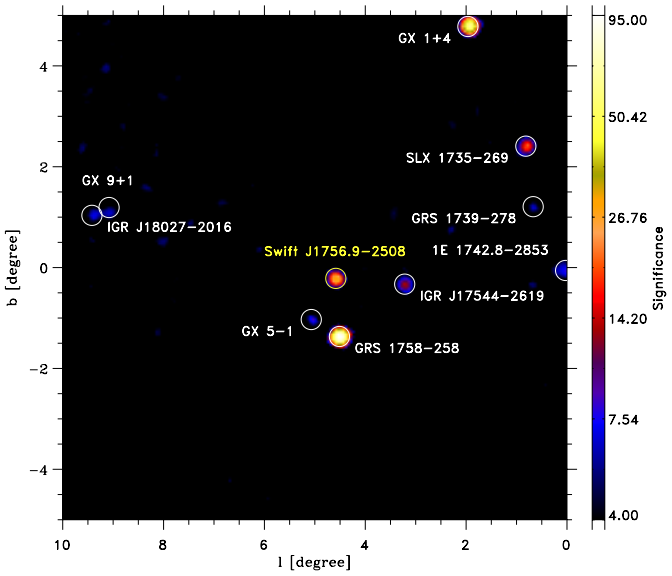

Fig. 1. INTEGRAL-ISGRI sky image in the 20–50 keV band (significance map, in Galactic coordinates (l, b)), of the field of view around the AMXP Swift J1756.9–2508 taken during time interval MJD 58209.35–58219.50 with an effective exposure time of 248 ks (rev. 1937, 1939, and 1940 combined). The source was detected with a significance of $\sim 30\sigma$.

The algorithms used for the spatial and spectral analysis are described in Goldwurm et al. (2003). We analyzed data from the IBIS-ISGRI coded mask telescope (Ubertini et al. 2003; Lebrun et al. 2003), at energies between 22 and 300 keV, and from the JEM-X monitor, module 1 and 2 (Lund et al. 2003) between 5 and 20 keV. Because most of the pointings were not aimed at Swift J1756.9–2508 as the primary target, the source was rarely within the JEM-X field of view of <3°.5. Therefore, we did not use the JEM-X data for the spectral analysis.

We show in Fig. 1 part of the ISGRI field of view for 20–50 keV energy range (significance map) centered on the position of Swift J1756.9–2508. The source was clearly detected in the mosaic at a significance of $\sim 30\sigma$ in the 20–50 keV energy range and still significant with $\sim 5.8\sigma$ in the higher 100–150 keV energy range. The best-determined position is at $\alpha_{J2000} = 17^{h}56^{m}57^{s}.35$ and $\delta_{J2000} = -25°06'27''.8$, with an associated uncertainty of 0'.5 at the 90% c.l. (20–50 keV; Gros et al. 2003).

We extracted the IBIS-ISGRI light curve of Swift J1756.9–2508 at the resolution of one ScW for the entire observational period covered by INTEGRAL (see Sect. 3). However, the ISGRI spectra were extracted only using the dedicated continuous ToO observation in revolution 1939, as these occurred nearly simultaneously with the NICER *NuSTAR* and *XMM-Newton* observations (see Sects. 2.2–2.4) and permitted the most accurate description of the source averaged broadband high-energy emission. The outburst profile is described in Sect. 3 and the averaged broadband spectrum of the source, as it was measured almost simultaneously by all these instruments, is described in Sect. 4. We note that INTEGRAL did not carry out observations of Swift J1756.9–2508 during its 2019 outburst.

2.2. NICER

The Neutron star Interior Composition ExploreR (NICER), launched on June 3, 2017, is an International Space Station payload dedicated to (spectral) timing studies in the 0.2–12 keV band at an unprecedented time resolution of ~100 ns (Arzoumanian et al. 2014). During the 2018 outburst, NICER started regular observations of Swift J1756.9–2508 on April 3, 2018 (MJD 58211.6; obs. ID 1050230101), namely, a few days after the detection by INTEGRAL, and it ended on April 25, 2018 (MJD 58233.8; obs. ID 1050230108) when the source reached undetectable levels. During the 2019 outburst, NICER observed Swift J1756.9–2508 seven times, including Obs. ID 2050230101 through 2050230107.

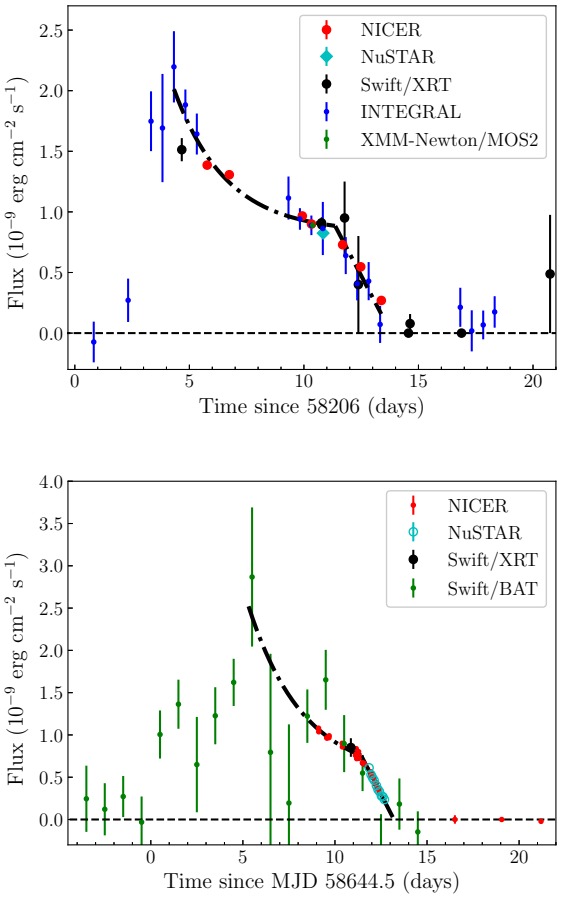

Fig. 2. Evolution of the bolometric fluxes (0.1–300 keV) of Swift J1756.9–2508 for the 2018 (*top panel*) and 2019 (*bottom panel*) outbursts; see Sect. 3 for more details. The dot-dash lines correspond to the best-fit exponential profile, $F \propto e^{-t/2.3\,\mathrm{d}}$ and $F \propto e^{-t/3\,\mathrm{d}}$, followed by a linear decay, respectively.

We carried out standard data processing using the NICER Data Analysis Software (NICERDAS). The default filtering criteria were applied to extract the cleaned event data. The spectra and light curves were obtained by `xselect`. The spectrum from obs. ID 1050230104 was used together with those from the other instruments in the 2018 outburst. The background spectrum is adopted from obs. ID 1050230107, when Swift J1756.9–2508 was in a quiescent state with negligible X-ray emission. In the pulse-profile analysis of the 2018 NICER data (see Sect. 5.2) we used obs. ID 1050230108 for the estimation of the background to obtain background corrected fractional amplitudes.

For the 2019 outburst, the NICER observation with obs. ID 2050230104 overlapped with the (single) *NuSTAR* observation. In order to obtain a simultaneous broadband spectrum, the data between MJD 58656.3485 and 58656.9060 were analyzed; in this case, the background spectrum was from obs. ID 2050230107. The redistribution matrix file and ancillary

response file were taken from the official webpage[2]. For details on the timing analysis of NICER data we refer to Sect. 5.

2.3. NuSTAR

NuSTAR observed Swift J1756.9–2508 on April 8, 2018 (Obs. ID 90402313002; MJD ~58216.4), April 14, 2018 (Obs. ID 90402313004; MJD ~58222.1), and on June 22, 2019 (Obs. ID 90501329001; MJD ~58656.3). The second observation during the 2018 outburst was carried out when Swift J1756.9–2508 returned into quiescent state, so it was not considered in this work. For the first 2018 observation, we cleaned the event file using the *NuSTAR* pipeline tool `nupipeline` for both FPMA and FPMB. The light curves and spectra were extracted from a circular region with a radius of 60″ centered on the location of Swift J1756.9–2508 (source region) by using `nuproducts`, and the response files were produced simultaneously. To extract the background spectra, we chose a source-free circular background region located on the same chip with a radial aperture of 60″.

In the timing analysis, we barycentered event data from the source region using `HEASOFT` multi-mission tool `barycorr v2.1`, with *NuSTAR* fine clock-correction file #110, yielding time tags accurate at 60–100 μs level (Bachetti et al. 2021). To obtain background corrected timing characteristics, such as fractional amplitudes, we used the above mentioned background region. For the observation carried out during the 2019 outburst, similar procedures were applied as for the 2018 outburst, except that the spectra were cut in the same interval as the NICER obs. ID 2050230104. For more details, see Sect. 2.2.

2.4. XMM-Newton

On April 8, 2018, *XMM-Newton* started an observation of Swift J1756.9–2508 (MJD 58216.07). The (imaging) EPIC-pn instrument (Strüder et al. 2001, 0.15–12 keV) on board *XMM-Newton* was operated in timing mode (TM), allowing for timing studies at a ~30 μs time resolution. The other (imaging) EPIC instrument equipped with two cameras, MOS-1 and MOS-2 (Turner et al. 2001), were set to full window (FW) and TM, respectively.

We ran the `XMM-SAS` pipeline analysis scripts (SAS-version 18.0) for all EPIC and RGS instruments on board *XMM-Newton*. We verified that the background flares were not detected, therefore, it was not necessary to perform further cleaning. We extracted the source spectrum from MOS-2 in TM from the `RAWX` interval [285, 325], while the background spectrum was extracted from MOS-2 in the image mode from a circle region with a radius of 150″. The response matrix file and ancillary response file were generated using `rmfgen` and `arfgen`, respectively.

For the timing analysis, we used data from the *XMM-Newton* EPIC pn. These were subsequently barycentered using the `SAS barycen 1.21` script. Furthermore, we selected the one-dimensional spatial parameter `RAWX` by defining the source-region as `RAWX` interval Ferrigno et al. (2011), Hartman et al. (2009) and the background region as the combination of `RAWX` Bult et al. (2018b), Cumming (2003) and Kuiper et al. (2020), Mazzola et al. (2018), chosen far from the source region. The latter has been used in the estimation of background corrected fractional amplitudes in the pulse-profile analysis.

The (non-imaging) Reflection Grating Spectrometers (RGS) (den Herder et al. 2001), on board *XMM-Newton*, operated in default mode (HighEventRate with Single Event Selection; HER + SES), collecting spectral information in the 0.35–2.5 keV band. Two RGS spectra were extracted using `rgsproc` and the corresponding response files were created using `rgsrmfgen`. In order to increase the signal-to-noise ratio (S/N), we combined the spectra of two RGS data in first order. *XMM-Newton* did not observe Swift J1756.9–2508 during its 2019 outburst.

2.5. Insight-HXMT

The first Chinese X-ray telescope, the Hard X-ray Modulation Telescope (HXMT), was launched on June 15, 2017 and later dubbed *Insight*-HXMT (Zhang et al. 2020). Three slat-collimated instruments, the Low Energy X-ray telescope (LE, 1–15 keV, 384 cm^2; Chen et al. 2020), the Medium Energy X-ray telescope (ME, 5–30 keV, 952 cm^2; Cao et al. 2020) and the High Energy X-ray telescope (HE, 20–250 keV, 5100 cm^2; Liu et al. 2020) on board *Insight*-HXMT provide the capability for the broadband X-ray timing and spectroscopy. *Insight*-HXMT observed Swift J1756.9–2508 during its 2018 outburst on MJD 58213.1–58213.8. We employed the HE and ME data to investigate the timing properties of the source because of their relatively good time resolution (~2 μs for HE, ~20 μs for ME). We analyzed the data using the *Insight*-HXMT Data Analysis Software package (HXMTDAS) version 2.01. The ME and HE data were calibrated by using the scripts `mepical` and `hepical`, respectively. The good time intervals were individually selected from the scripts `megtigen` and `hegtigen` with the loose criteria, that is, ELV > 0 and the satellite located outside the SAA region. Finally, the events were obtained using `mescreen` and `hescreen` and were barycentered by the tool `hxbary`. *Insight*-HXMT did not observe Swift J1756.9–2508 during its 2019 outburst.

2.6. Swift

In total, nine and one observations, respectively, are available for the 2018 and 2019 outbursts from *Swift*/XRT, respectively. The *Swift*/XRT light curves were only reduced to construct the outburst profiles during the 2018 and 2019 outbursts. We reduced the *Swift*/XRT data in the photon counting mode. The pipeline `xrtpipeline` was operated for each observation and the light curve was extracted from a circle region centered on the source position with a radius of 25″ and corrected by the *Swift* tool `xrtlccorr`.

3. The outburst profiles

The light curves of Swift J1756.9–2508, as obtained from all available X-ray data, show the entire 2018 and 2019 outbursts both lasting about 15 d (from March 31 to April 14, 2018 and June 10 to 25, 2019) are shown in Fig. 2. Because the 2019 outburst was observed at the last stage during its decay phase, the flux in one-day bins was estimated using the *Swift*-BAT data. The count-rates measured from all instruments were converted to bolometric flux (0.1–300 keV) using the spectral analysis results obtained in Sect. 4 for the respective outbursts.

The profile of the outburst observed from Swift J1756.9–2508 is not too dissimilar from those shown by other AMXPs, which are typically characterized by a swift rise time (~2–3 d), followed by ~7 d exponential and ~2 d linear decay down to the quiescence level (see e.g., Falanga et al. 2005a, 2011, 2012; Ferrigno et al. 2011; Bozzo et al. 2016; De Falco et al.

[2] https://heasarc.gsfc.nasa.gov/docs/nicer/tools/nicer_bkg_est_tools.html

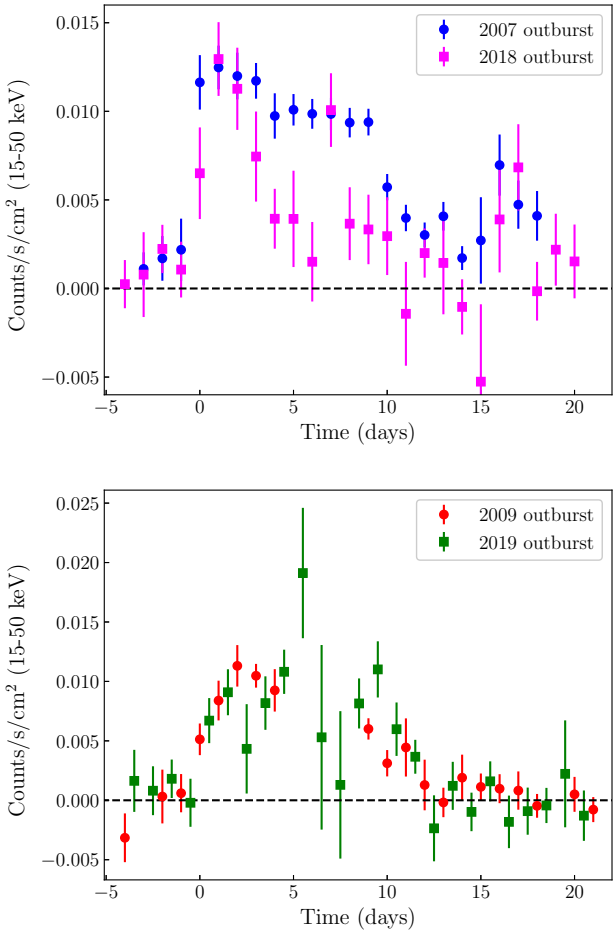

Fig. 3. *Swift*-BAT daily averaged (15–50 keV) profiles of the 2007 (blue dots) and 2018 (magenta squares) outbursts (*top panel*), the 2009 (red dots), and 2019 (greed squares) outbursts (*bottom panel*) from Swift J1756.9–2508. The start time of the 2007, 2009, 2018, and 2019 outbursts are MJD 54258, 55012, 58208, and 58644.5, respectively.

2017a,b; Kuiper et al. 2020). Using the best covered 2018 outburst profile, we estimate the outburst peak flux around $\sim 2.0 \times 10^{-9}$ erg cm^{-2} s^{-1} in the 0.1–300 keV energy range (see Fig. 2); this value is similar to that for all other observed outbursts, considering the same energy band (Krimm et al. 2007a; Linares et al. 2008; Patruno et al. 2009a; Sanna et al. 2018c).

Such outbursts are typically described by the disk instability model (see King & Ritter 1998, for more details), which predicts that both linear and exponentially decaying outbursts can be produced. Typically, for such outbursts, the flux decays from the maximum exponentially until it reaches a break ("knee"), in our case around MJD 58217 (2018 outburst) or MJD 58656 (2019 outburst), and then linearly drops to the quiescent level. Following Powell et al. (2007), the outer disk radius can be estimated by fitting the decay profile (see Fig. 2) with the expression:

$$L_X = (L_t - L_e)\ \exp[-(t - t_t)/\tau_e] + L_e, \quad (1)$$

where L_e (the limit luminosity of the exponential decay), t_t (the break time), L_t (the luminosity at the break time t_t), and τ_e (exponential decay time) are all free parameters. The outer disk radius is $R_{\rm disk}(\tau_e) = (\tau_e\, 3\nu_{\rm KR})^{1/2} \sim 2.5 \times 10^{10}$ cm, where the value of the viscosity near the outer disk edge $\nu_{\rm KR} = 10^{15}$ cm^2 s^{-1} is adopted (see King & Ritter 1998; Powell et al. 2007, for more details). In the 2019 outburst, we obtain the outer disk radius of $R_{\rm disk} \sim 3.0 \times 10^{10}$ cm. For the binary inclination of 60° and the NS mass of 1.4 $M_\odot$, the companion mass M_c is 0.0078 $M_\odot$. We adopted the relation

$$\frac{b_1}{a} = 0.741 - 1.682q + 12.053q^2 - 42.342q^3 - 0.0663 \log_{10} q, \quad (2)$$

where b_1 is the distance between the NS and the Lagrange point, L_1, of the binary system and a is the binary separation, which has an accuracy of 0.5% for q between 0.0025 and 0.11 (Iaria et al. 2021). The circularization radius $R_{\rm circ}$ can be estimated from (see e.g., Frank et al. 2002):

$$\frac{R_{\rm circ}}{a} = (1 + q)(b_1/a)^4. \quad (3)$$

We found that the outer disk radii in the 2018 and 2019 outbursts satisfy the condition $R_{\rm circ} < R_{\rm disk} < b_1$, where $R_{\rm circ} \approx 2.3 \times 10^{10}$ cm and $b_1 \approx 3.3 \times 10^{10}$ cm.

In Fig. 3, an inspection of all the *Swift*-BAT outburst data shows that the period of activity in 2018–19 broadly follows the pattern of the previous outbursts, with two more closely-spaced outbursts separated by a longer interval. The 2009 outburst followed the discovery outburst in 2007 by 2.1 yr; the 2019 outburst came 1.2 yr after 2018. However, the 2018 outburst came after a much longer quiescent interval, of 8.7 yr.

Such pairs of outbursts have only previously been observed from the low-mass X-ray binaries IGR J00291+5934 and XTE J1118+480 (Hartman et al. 2011), although in those systems, the inter-outburst separation was 30 d. Those authors attributed the secondary outburst to leftover material in the accretion disk that was not deposited on the NS during the first outburst. The atypical mass distribution left in the disk when the accretion stalls during the first outburst, leads to the unusual slow-rise shape of the second outburst; this pattern is very similar to what is observed in Swift J1756.9–2508.

Similarly, for those sources, the wide variation in outburst separation in Swift J1756.9–2508 is not consistent with a steady accretion rate into the disk, unless the bulk of the fuel for the second outburst in each pair was leftover material that was not accreted during the first outburst. We estimate here the fraction of fuel leftover, and the lower limit on the steady accretion rate, as follows. By integrating the flux measurements over each outburst, the fluences for the 2018 and 2019 outbursts are 1.1×10^{-3} erg cm^{-2} and 1.2×10^{-3} erg cm^{-2}, respectively. The fluence of each outburst arises from an accreted mass of:

$$\Delta M = \frac{4\pi d^2 \int F_X {\rm d}t}{Q_{\rm grav}} \approx \frac{4\pi d^2 R_{\rm NS} \int F_X {\rm d}t}{G M_{\rm NS}}, \quad (4)$$

where $Q_{\rm grav} \approx GM_{\rm NS}/R_{\rm NS}$ is the gravitational potential energy liberated during accretion. For each of the 2018 and 2019 outbursts, the accreted mass is $\Delta M \approx 3 \times 10^{-11}\ M_\odot d_8^2 r_{10} m_{1.4}^{-1}$, where d_8 is the distance in units of 8 kpc, r_{10} the NS radius in units of 10 km, and $m_{1.4}$ the NS mass in units of $1.4 M_\odot$. Assuming a constant accretion rate $\dot{M}$ over the interval between the 2009 and 2019 outbursts, we can solve for this quantity as well as the amount of fuel left over following the 2018 outburst. We find a steady accretion rate of $5 \times 10^{-12}\ M_\odot$ yr$^{-1} d_8^2 r_{10}\, m_{1.4}^{-1}$, implying about 45% of the material in the disk remaining after the end of the 2018 outburst.

We can estimate a lower limit for the distance to the source by equating the implied long-term accretion rate above, with the expected accretion rate driven by gravitational-wave radiation from the binary orbit (e.g. Bildsten & Chakrabarty 2001). Adopting the minimum companion mass of $M_c = 6.7 \times 10^{-3}\ M_\odot$

Table 2. Best parameters determined from the fits to the broadband emission spectra of Swift J1756.9–2508 using the PHABS absorbed comptonization model COMPPS.

Parameter	Unit	2018 outburst	2019 outburst
$N_{\rm H}$	(10^{22} cm^{-2})	4.29 ± 0.05	4.17 ± 0.12
$kT_{\rm bb,seed}$	(keV)	0.79 ± 0.01	0.67 ± 0.02
$kT_{\rm e}$	(keV)	41.6 ± 0.7	44.6 ± 1.3
τ_T		1.44 ± 0.02	1.23 ± 0.03
$K_{\rm bb}$	(km^2)	150 ± 9	156 ± 20
$\chi^2_{\rm red}$/d.o.f.		1.11/1644	1.01/858
$F_{\rm bol}$ [(a)]	(10^{-10} erg cm^{-2} s^{-1})	8.63 ± 0.06	4.44 ± 0.05

Notes. In the 2018 outburst, the spectra were obtained from the *XMM-Newton*, NICER, *NuSTAR*, and INTEGRAL. The NICER and *NuSTAR* spectra were utilized for the 2019 outburst. Uncertainties are given at 1σ confidence level. [(a)]Unabsorbed flux in the 0.1–300 keV energy range.

for a $1.4 M_\odot$ NS Krimm et al. (2007b), we find that $d_8^2 \gtrsim 0.277\, m_{1.4}^{5/3}\, r_{10}^{-1}$, so that $d \gtrsim 4$ kpc. This limit is consistent with our assumed distance of 8 kpc.

4. Broadband spectral analysis of the 2018 and 2019 outbursts

We studied the broadband X-ray spectra of the 2018 and 2019 outbursts individually. For the 2018 outburst, we fit the quasi-simultaneous spectra, including the INTEGRAL-ISGRI (20–250 keV) ToO data between MJD 58215.8–58216.8, the *NuSTAR* FPMA/FPMB (3.5–79 keV) data starting on MJD 58216.4 (obs. ID 90402313002), NICER (1.5–10 keV) data starting on MJD 58216.0 (Obs. ID 1050230104), *XMM-Newton* MOS (2–10 keV), and RGS (1–2.4 keV) data starting on MJD 58216.1. We note that the MOS spectrum showed a strong excess below 2 keV, which may be affected by the straylight. For the 2019 outburst, we consider the simultaneous observations from NICER (1.5–10 keV, Obs. ID 2050230104) and *NuSTAR* FPMA/FPMB (3–79 keV, Obs. ID 00033646004), respectively. All spectra are grouped to make sure that each channel has more than 25 photons. For each instrument, a multiplication factor is included in the fit to account for the uncertainty in the cross-calibration of the instruments. For all fits, the factor is fixed at 1 for the *NuSTAR* FPMA instrument. All uncertainties in the spectral parameters are given at a 1σ confidence level for a single parameter. The spectral analysis were carried out using Xspec version 12.10 (Arnaud et al. 1996).

We fit all the spectra by using the thermal Comptonization model, COMPPS, in the slab geometry (Poutanen & Svensson 1996), with the interstellar absorption described by model `phabs`. This model has been used previously to fit the broadband spectra of AMXPs (see e.g., De Falco et al. 2017b,a; Li et al. 2018; Kuiper et al. 2020, and references therein). The main parameters are the Thomson optical depth across the slab, τ_T, the electron temperature, $kT_{\rm e}$, the temperature of the soft seed photons (assumed to be injected from the bottom of the slab), $kT_{\rm bb,\ seed}$, the normalization factor for the seed blackbody photons, $K_{\rm bb} = (R_{\rm km}/d_{10})^2$ (with d_{10} being distance in units of 10 kpc), and the inclination angle θ (fixed at 60°) between the slab normal and the line of sight to the observer. The interstellar absorption is described by the hydrogen column density, $N_{\rm H}$. The best-fit parameters for all models are reported in Table 2. For the distance of 8 kpc, the size of the blackbody emitting region $R_{\rm bb} = 0.8\sqrt{K_{\rm bb}} \approx 10$ km. This is very similar to IGR J17498−2921 (Falanga et al. 2012), which was also assumed to be situated at the same distance, but much larger, for instance, than in XTE J1751−305 (Gierliński & Poutanen 2005). Such a large size is hardly consistent with the hotspot at the NS surface and might indicate that the distance to the source is smaller. The bolometric fluxes are calculated by the convolution model `cflux` in the 0.1–300 keV energy range. In Fig. 4, we show the best-fit spectra.

We find that all multiplication cross-calibration factors are around unity, which means the flux calibration of these instruments is well established and the source did not vary much between the quasi-simultaneous observations. The 2018 and 2019 outbursts can be characterized by similar hard spectra (see Table 2). This indicates that even thought the 2019 outburst was observed at a later outburst stage, namely, at a flux level lower by a factor 1.9, the decay of the outburst is characterized by a nearly constant spectral shape described by similar electron temperature, $kT_{\rm e}$, soft seed photons temperature, $kT_{\rm bb,\ seed}$, and the optical depth, τ_T. The spectral parameters are similar to those of many other AMXPs (see e.g., Falanga et al. 2011, and references therein). The spectra for the 2018 and 2019 outbursts in narrower energy ranges are well described by a power-law with a photon index in the range of ∼1.8–2.0, which is compatible to those measured in the 2007 and 2009 outbursts (Krimm et al. 2007a; Linares et al. 2008; Patruno et al. 2009a). Also, the hydrogen column density was similarly high, namely, $N_{\rm H} \sim (4.5\text{–}5.4) \times 10^{22}$ cm^{-2}. This also confirms that all four observed outbursts are very similar (see also Sect. 3). We note that our estimate of the blackbody normalization is at least factor of 30 larger than the normalization quoted by Sanna et al. (2018c), who used a phenomenological blackbody plus cutoff power-law model. The difference comes from the facts that in the COMPPS model, only a small fraction, that is, $\exp(-\tau_T/\cos\theta) \sim 0.06$, of the seed blackbody photons pass through the Comptonizing slab unaffected; the rest is scattered and produce the hard tail extending to 100 keV. Also, in our model, a large fraction of the flux below 3 keV comes from the blackbody, whereaws in the model of Sanna et al. (2018c), the power law contributes most of the flux.

5. Timing analysis

Irrespective of the instrument, in timing analyses, we had to convert the Terrestial Time (TT) arrival times of the (selected) events to arrival times at the solar system barycenter (in a TDB time scale). For this process, throughout in this work we used: 1) the JPL DE405 solar system ephemeris; 2) the instantaneous spacecraft position with respect to the Earth's center; and 3) the X-ray celestial position of Swift J1756.9–2508, $\alpha_{\rm J2000} = 17^{\rm h}56^{\rm m}57\overset{\rm s}{.}35$ and $\delta_{\rm J2000} = -25°06'27\overset{''}{.}8$ obtained by the *Swift*-XRT telescope (Krimm et al. 2007b).

5.1. NICER timing analysis of the 2018 and 2019 outbursts

For our timing analysis, we selected "cleaned" barycentered NICER XTI events, collected during the 2018 and 2019 outbursts, from the standard pipeline analysis with measured energies between 0.5 and 10 keV. Events with energies between 12–15 keV, however, were used to flag periods with high-background levels (e.g., South Atlantic Anomaly ingress or egress, etc.) as bad, and these intervals have been ignored in further analyses. Moreover, events from noisy or malfunctioning detectors were ignored. The screened events were subsequently barycentered using a (multi-instrument serving) IDL procedure.

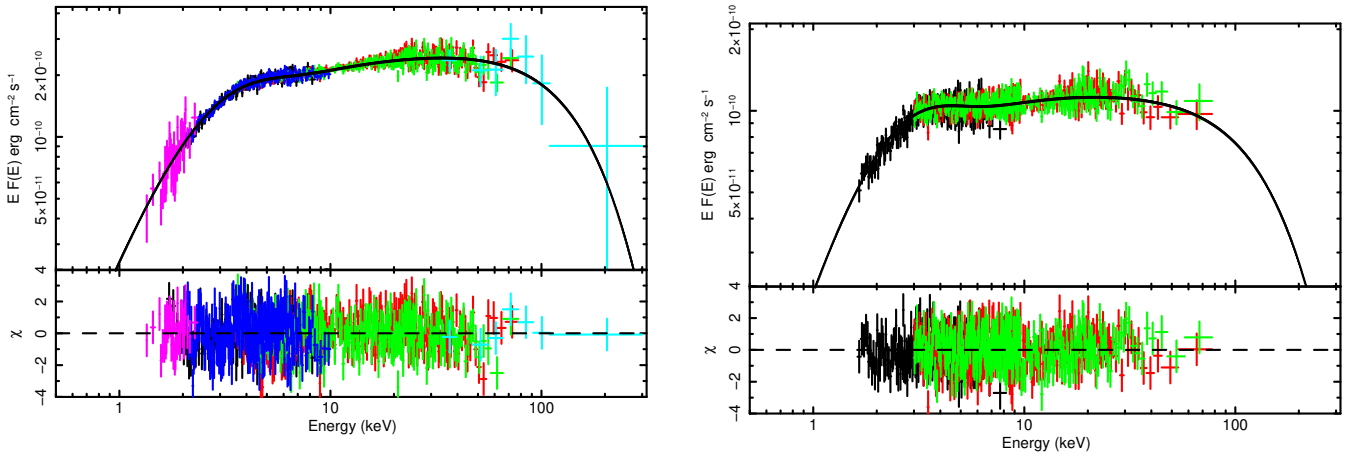

Fig. 4. Unfolded and unabsorbed broadband spectra of Swift J1756.9–2508. *Left panel:* spectrum for the 2018 outburst in the 1–250 keV energy range. The data points are obtained from the combined of two *XMM-Newton* RGS instruments (magenta datapoints, ∼1.2–2.4 keV), *XMM-Newton* EPIC-MOS2 (blue points, 2–10 keV), NICER (black points, 1.5–10 keV) *NuSTAR* FPMA/FPMB (red and green points, 3.5–80 keV), and INTEGRAL-ISGRI (cyan points, 30–250 keV). *Right panel:* spectrum of the 2019 outburst in the 1.5–80 keV energy range. The data points are obtained from the NICER (black points, ∼1.5–10 keV), *NuSTAR* FPMA/FPMB (red and green points, 3–80 keV). In both cases, the fits are obtained with the COMPPS model, represented with a solid line. The residuals from the best fit are shown at the bottom.

Table 3. Positional, rotational, and orbital parameters used from other works and derived in this work for Swift J1756.9–2508.

Parameter	Units	Values
α_{2000}		$17^{\rm h}56^{\rm m}57\overset{\rm s}{.}350$
δ_{2000}		$-25°06'27\overset{''}{.}80$
JPL Ephemeris		DE405
$P_{\rm orb}$	s	3282.3515
$a_x \sin i$	lt-s	0.00597
e		0.00
	Outburst – 2018	
ν	Hz	182.065 803 84(3)
Epoch, t_0	MJD; TDB	58216.0
Validity range	MJD; TDB	58211−58219
$T_{\rm asc,2018}$	MJD; TDB	58211.017 52(6)
	Outburst – 2019	
ν	Hz	182.065 803 4(2)
Epoch, t_0	MJD; TDB	58654.0
Validity range	MJD; TDB	58653−58657
$T_{\rm asc,2019}$	MJD; TDB	58655.996 57(12)

For each outburst, we individually determined the pulse frequency, ν, and time of ascending node, $T_{\rm asc}$, in a 2d-optimization scheme based on a SIMPLEX algorithm (see, e.g., De Falco et al. 2017b; Kuiper et al. 2020, for more details), finding the global maximum of the $Z^2(\phi)$-test statistics (Buccheri et al. 1983). In this approach we kept the orbital period, $P_{\rm orb}$, projected semi major axis, $a_x \sin i$, fixed at the optimum values given by Patruno et al. (2010) (see their Table 4). We verified that using updated orbital ephemeris information (Bult et al. 2018a) had no impact on the $T_{\rm asc}$ values derived here. The best fit values for ν and $T_{\rm asc}$, along with the validity interval and epoch t_0 for both outbursts, are individually listed in Table 3 and are used later in this work in estimating the orbital period derivative combining information from all registered outbursts (see Sect. 6). Equipped with accurate timing models for both outbursts (see Table 3), we phase-folded the barycentered event times from different instruments for different energy bands both for the 2018 and 2019 outbursts. The results are shown in Figs. 5 and 6 for the 2018 and 2019 outbursts, respectively.

During the 2018 (also for the 2019) outburst, no pulsed emission was detected below 1 keV using NICER and *XMM-Newton* data. *NuSTAR* detected pulsed emission up to ∼60 keV during the 2018 outburst. Folding INTEGRAL-ISGRI barycentered data of the 2018 outburst for the 20–60 keV band did not result in a detection of the pulsed emission in line with the expectations given the moderate total outburst flux, low exposure, and low pulsed fraction of $\lesssim$8% (see Sect. 5.2). However, with the *Insight*-HXMT HE instrument, significant pulsed emission has been detected up to ∼100 keV (see lower right panel of Fig. 5) in spite of relatively low exposure. This suggests great prospects for future observations with *Insight*-HXMT of the AMXP outbursts.

5.2. Harmonics analysis: Pulsed amplitudes and phase lags

We produced pulse-phase distributions in narrow energy bands for NICER, *XMM-Newton*, and *NuSTAR*, covering the ∼1–60 keV band, to obtain quantitative information about morphology changes of the pulse-profile as a function of energy. For this purpose, we fit these measured distributions $\mathcal{N}(\phi)$ with a truncated Fourier series given by

$$\mathcal{F}(\phi) = A_0 + \sum_{k=1}^{n} A_k \cos[k\,(\phi - \phi_k)]. \quad (5)$$

For each harmonic, the maxima occur at $\phi_{\rm max} = \phi_k \bmod (2\pi/k)$ (in radians).

The results of these fits are shown in Fig. 7. The left panel shows the fractional amplitude, A_k/A_0, and the right panel the phase angle, ϕ_k, converted from radians to pulse phase, for both the fundamental ($k = 1$, in black) and the first overtone ($k = 2$, in red). The different symbols indicated different instruments (NICER, 1–10 keV, squares; *XMM-Newton* EPIC-pn 1–12 keV, circles, and *NuSTAR*, 3–60 keV, triangles). The pulsed fraction of the fundamental component increases from ∼4% up to ∼7.5% from 1 to 5 keV, from where it more or less saturates at a level of ∼7.5%. The first overtone fluctuates around 3.5% with an indication for a depression down to ∼1% around 12 keV. These results

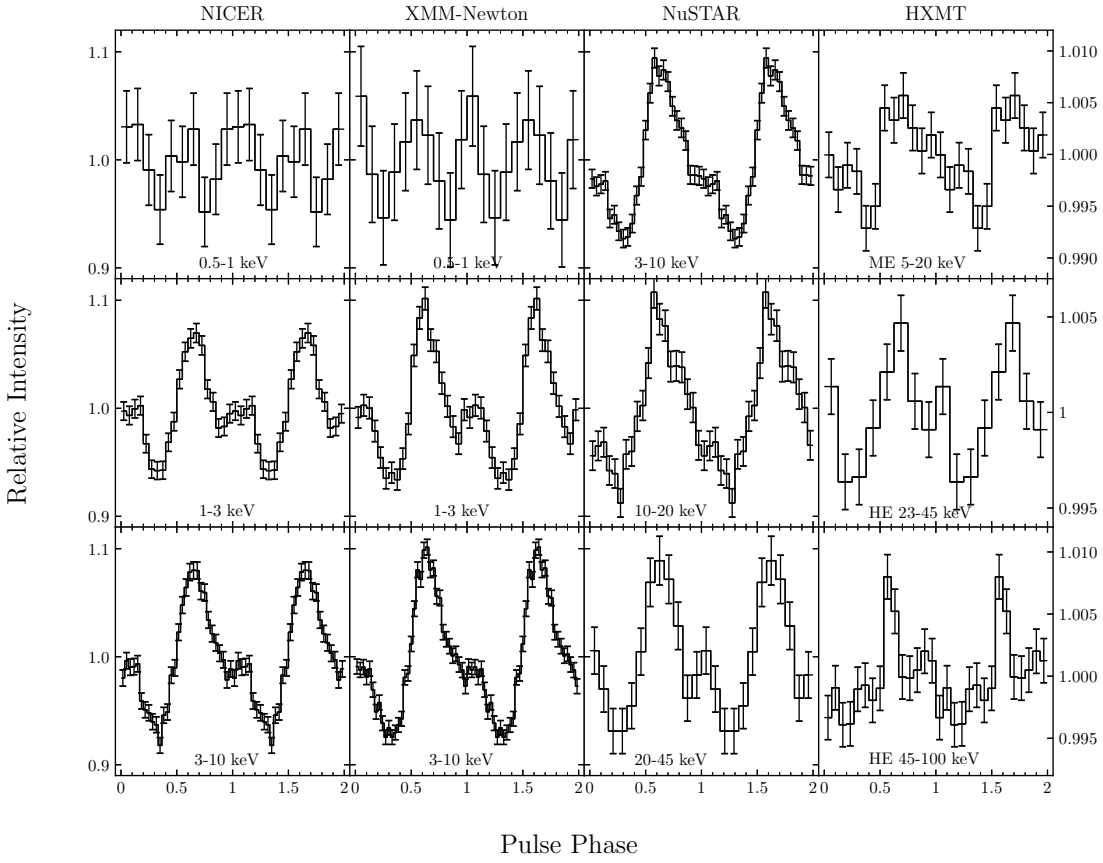

Fig. 5. Pulse profiles of Swift J1756.9–2508 observed by NICER, *XMM-Newton*, *NuSTAR*, and *Insight*-HXMT during the 2018 outburst.

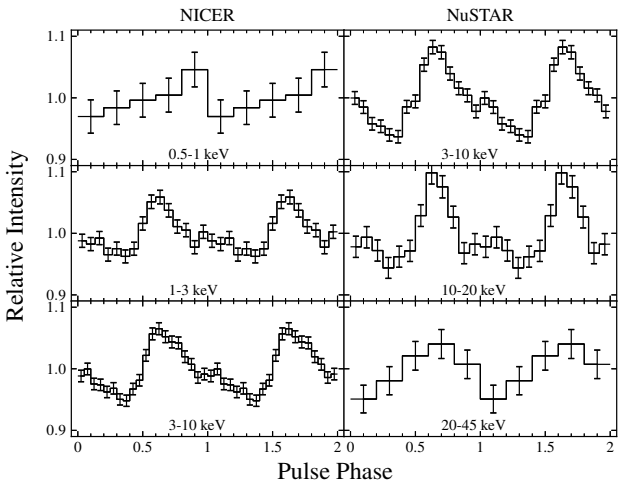

Fig. 6. Pulse profiles of Swift J1756.9–2508 observed by NICER and *NuSTAR* during the 2019 outburst.

are consistent with those reported by Sanna et al. (2018c) (e.g. their Fig. 5). Such a behavior was also observed in other sources (see, e.g., Patruno et al. 2009b) and is likely related to an increasing contribution of an unpulsed emission from the accretion disk. The phase angle plot (Fig. 7 right panel) shows that the location of both harmonics is stable up to at least 10 keV (see also bottom panel of Fig. 2 of Bult et al. 2018a, for equivalent results), aside from the occurence of a possible small drift to smaller values: from 0.7 to 0.65 for the fundamental and from 0.12 to 0.07 for the first overtone.

6. Orbital period

From the outburst in 2019, we have an additional well-determined $T_{\rm asc}$ value. It allows us to perform a coherent analysis of the orbital period evolution across a longer baseline, as compared with Bult et al. (2018a) and Sanna et al. (2018c). Following the procedure introduced in Hartman et al. (2008), we calculate the residual time of passage through the ascending node:

$$\Delta T_{\rm asc} = T_{{\rm asc},\,i} - (T_{\rm ref} + NP_{\rm orb}), \tag{6}$$

where $T_{{\rm asc},\,i}$ is the time of ascending node determined from the i-th outburst, $T_{\rm ref}$ is the reference time, N is the integer number of orbital cycles between the ith outburst and $T_{\rm ref}$, and $P_{\rm orb}$ is the orbital period. We use the orbital period reported in Table 3 and the reference time $T_{\rm ref}$ as the time of ascending node in the 2007 outburst (Krimm et al. 2007b) to obtain the values of $\Delta T_{\rm asc}$ for four outbursts. The errors of $\Delta T_{\rm asc}$ are from the uncertainties of $T_{\rm asc}$. In Fig. 8, we fit the $\Delta T_{\rm asc}$ evolution with a parabolic function, and obtain a best fit value of the orbital period derivative $\dot{P}$ of $(7.9 \pm 9.5) \times 10^{-13}$ s s^{-1}, which is consistent with the results reported in Sanna et al. (2018c) and Bult et al. (2018a). Hence, we conclude that the binary is well described by a constant period over a time span of nearly twelve years.

7. Non-detection of type-I X-ray bursts

We searched for type-I X-ray bursts in all available Swift J1756.9–2508 light curves during its 2018 and 2019 outbursts and detected none. The non-detection is consistent with the observations covering the 2007 and 2009 outbursts

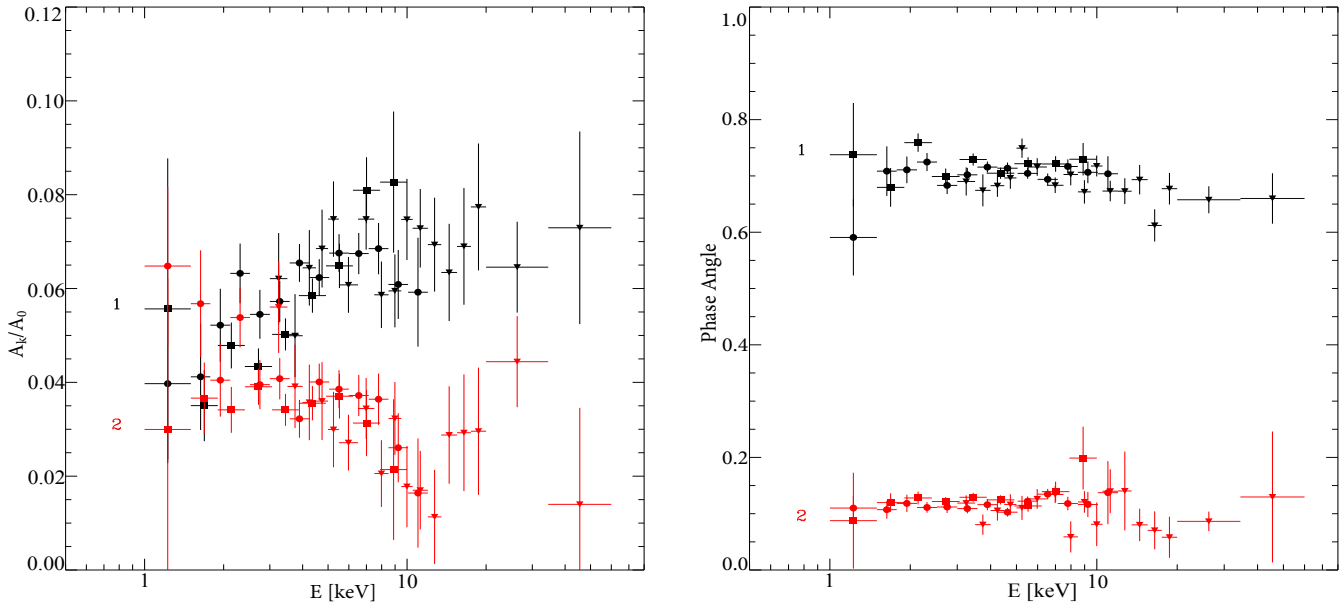

Fig. 7. Results of pulsed amplitudes and phase angles. *Left panel:* fractional amplitude of two harmonics (1 – fundamental, 2 – first overtone) as a function of energy using background corrected data from NICER (squares), *XMM-Newton* EPIC-pn (circles) and *NuSTAR* (triangles). The pulsed fraction of the fundamental component increases from ∼4% till ∼7.5% from 1 to 5 keV, from where it more or less saturates at a level of ∼7.5%. *Right panel:* phase angles ϕ_k (divided by 2π) for the two Fourier components as function of energy. They remain remarkably stable across the 1–60 keV band, with possibly a small drift for ϕ_1 to slightly lower values at energies above ∼10 keV.

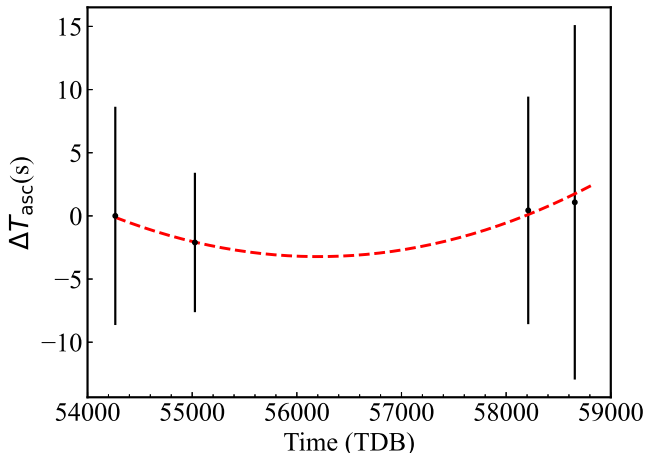

Fig. 8. Orbital period evolution of Swift J1756.9–2508 determined from the time of passage at the ascending node during its four outbursts. The red dashed line is the best fit parabolic model.

(Patruno et al. 2009a; Sanna et al. 2018c; Bult et al. 2018a; Rai & Paul 2019).

The non-detection of bursts in Swift J1756.9–2508 is likely a consequence of a low burst rate coupled with a low observational duty cycle in the X-ray observations, such that any bursts that might occur would fall within data gaps. The thermonuclear burst rate depends on the composition of the accreted fuel and the local mass accretion rate, $\dot{m}$, which, in turn, determine how much fuel must be accreted prior to ignition and the ignition depth. The known AMXPs can be divided into two distinct groups based on their orbital periods; either around 40 min or within the range of 2–11 h (see e.g., Campana & Di Salvo 2018). Stellar evolution models predict that AMXPs with an orbital period longer than one hour should host a highly evolved, hydrogen-rich brown dwarf companion star, and the heating from steady burning of the accreted H fuel prior to ignition will lead to burst recurrence times of hours to days (see e.g., Galloway & Cumming 2006; Heger et al. 2007; Falanga et al. 2011; Ferrigno et al. 2011; De Falco et al. 2017b,a; Li et al. 2018; Kuiper et al. 2020). However, "ultracompact" X-ray binaries (UCXBs) with orbital periods <80 min are expected to have low-temperature C, O or He white dwarf companions, that is, hydrogen-poor, highly evolved dwarfs (Deloye & Bildsten 2003). The mass-radius relation of AMXPs are shown in Fig. 9, by the assumption of a Roche lobe-filling companion (Paczyński 1971). The corresponding M_c versus R_c relations for different stellar evolution models are also provided in Fig. 9. The expected burst recurrence time for such systems, even if reaching the same accretion rates during outbursts as the H-rich systems, are substantially lower, significantly reducing the chance of detecting bursts (e.g., Cumming 2003).

We can roughly estimate the likely burst recurrence time based on the persistent flux of the source during the outburst The local mass accretion rate per unit area onto the NS is $\dot{m} = 4\pi d^2 F_{\rm bol}(1+z)(4\pi R_{\rm NS}^2(GM_{\rm NS}/R_{\rm NS}))^{-1}$, i.e., $\dot{m} \approx 3.7 \times 10^3 d_8^2\,{\rm g\,cm^{-2}\,s^{-1}}$ and $\dot{m} \approx 1.9 \times 10^3 d_8^2\,{\rm g\,cm^{-2}\,s^{-1}}$ for the 2018 and 2019 outbursts, respectively. If the accreted matter is pure helium, the expected recurrence time for type-I X-ray bursts is $t_{\rm rec} \approx y/\dot{m} \approx 116\,{\rm d}\,(y/10^{10}\,{\rm g\,cm^{-2}})(\dot{m}/10^3\,{\rm g\,cm^{-2}\,s^{-1}})^{-1}$, where y is the ignition depth of a helium burst (see e.g., in't Zand et al. 2007). For Swift J1756.9–2508, during its 2018 and 2019 outbursts, we estimate a burst recurrence time at the peak of the outburst of 30 d, longer than the total duration of the outbursts. If the accreted matter is composed of C and O, the X-ray bursts would be expected to occur at even larger ignition depths. We expect that the recurrence time should be much longer. Given recurrence times in excess of the outburst duration, it is questionable whether sufficient material would accrete to produce even a single burst.

While no type-I burst events were detected during outbursts of transient ultracompact AMXPs, including Swift J1756.9–2508, we note that some UCXBs can sustain accretion

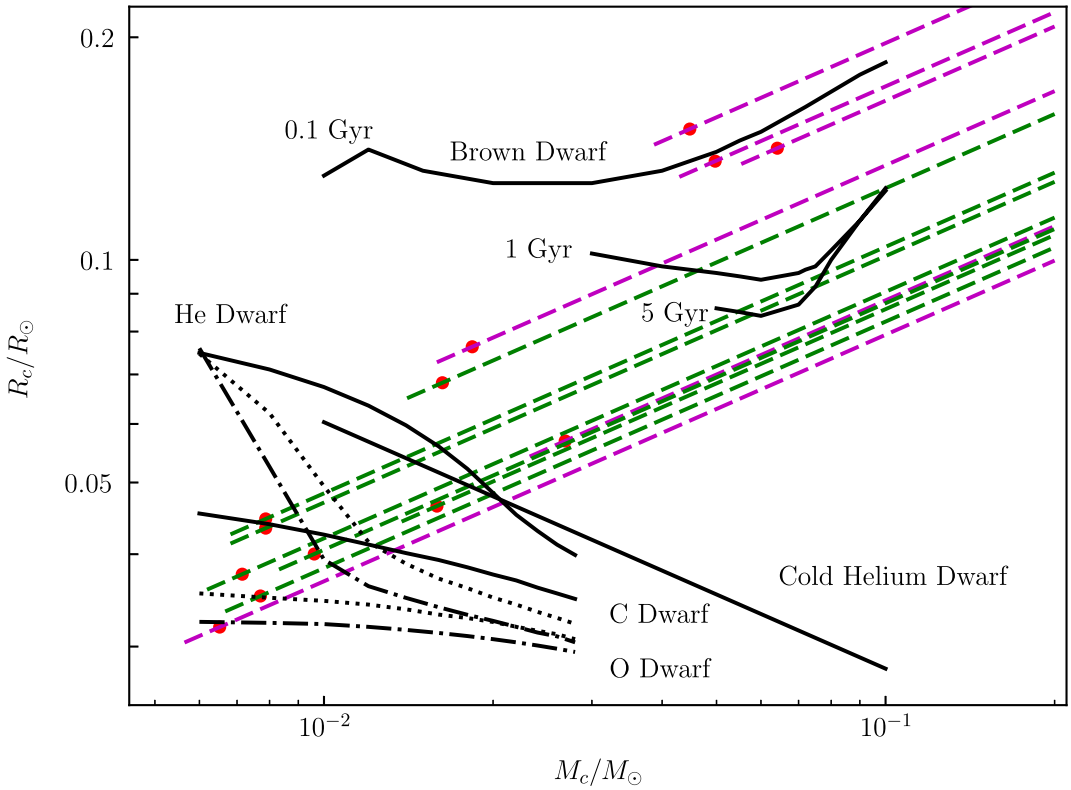

Fig. 9. Assumption of a Roche lobe-filling companion implies a mass-radius relation $R_c = 0.082\,(M_c/0.1\,M_\odot)^{1/3}(P_{orb}/40\text{ min})^{2/3}\,R_\odot$, shown in logarithmic scale for different AMXPs with orbital periods around 40 min. From bottom up, the sources are IGR J17062−6143 (Strohmayer et al. 2018), XTE J1807−294 (Campana et al. 2003), XTE J1751−305 (Papitto et al. 2010), XTE J0929−314 (Galloway et al. 2002), MAXI J0911−655 (Sanna et al. 2017), IGR J16597−3704 (Sanna et al. 2018a), Swift J1756.9–2508 (Krimm et al. 2007b), NGC 6440 X-2 (Altamirano et al. 2010), IGR J17494−3030 (Ng et al. 2021), HETE J1900.1−2455 (Kaaret et al. 2006), IGR J17379−3747 (Sanna et al. 2018b), SAX J1808.4−3658 (Wijnands & van der Klis 1998), and IGR J00291+5934 (Galloway et al. 2005). The magenta dashed lines show the AMXPs with detected type-I X-ray bursts, while the green dashed lines show the AMXPs without type-I X-ray bursts. The red points mark the inclination angle at 60°. We note that from all AMXPs with the orbital period shorter than 1 hr, except MAXI J0911−655 and IGR J17494−3030, no type-I X-ray bursts were detected. We also show the mass-radius relations for low mass regime H-poor dwarf equation of states for O (dot-dash lines), C (dotted lines), and He (solid lines) as well as low (10^4 K, lower lines) or high (3×10^4 K, upper lines) central temperatures.

persistently and exhibit type I bursts (e.g Cumming 2003; in't Zand et al. 2007; Falanga et al. 2008). This property may explain the recent detection of a presumed type I X-ray burst in the AMXP MAXI J0911−655 (Nakajima et al. 2020; Bult et al. 2020), and two intermediate duration X-ray bursts in IGR J17062−6143 (Degenaar et al. 2013; Keek et al. 2017). The transient AMXPs spend most of the time in a quiescent phase, with X-ray luminosities of 10^{31}−10^{33} erg s^{-1} corresponding to accretion rates that are likely far too low to produce thermonuclear bursts.

8. Summary

In this work, we analyze all public high-energy data and report the outburst profiles and the spectral and timing properties of Swift J1756.9–2508 observed by INTEGRAL, *XMM-Newton*, *NuSTAR*, NICER, and *Insight*-HXMT, during its 2018 and 2019 outbursts. We found these two outbursts showed quite similar behavior in several aspects. The outburst profiles showed a similar shape, which can be explained by the disk instability models. The broadband spectra – in the energy range of 1–250 keV for the brighter 2018 outburst and in the range of 1.5–80 keV for the fainter 2019 outbursts – were well fitted by the thermal Comptonization model CompPS with a similar set of parameters: the electron temperature kT_e = 40–50 keV, Thomson optical depth $\tau \sim 1.3$, and blackbody seed photon temperature $kT_{bb,seed} \sim 0.7$–0.8 keV. The spectral shape is very similar to those observed in many other AMXPs (Papitto et al. 2020).

We performed a coherent timing analysis for the 2018 and 2019 outbursts together. Pulsed emission has been detected from Swift J1756.9–2508 in the energy range of 1–10 keV using NICER and *XMM-Newton* data, in 3–60 keV using *NuSTAR* during both outbursts, and in the 5–100 keV range using *Insight*-HXMT during the 2018 outburst. We detected an increase of the pulse fraction from 4% to 7.5% from 1 to 5 keV saturating at higher energies. We found no evidence for a change in the spin frequency from our data set. Comparing the observed times of ascending node passage with the predicted values, we concluded that the binary system had a constant orbital period since the first outburst in 2007.

Swift J1756.9–2508 is the third LMXB that has exhibited pairs of closely-spaced outbursts, which (assuming a steady accretion rate onto the disk) must arise from incomplete accretion of the fuel accumulated in the disk, during the first outburst Hartman et al. (2011). Those authors explained the outburst pairs observed in IGR J00291+5934 as the result of a "quasi-propeller" regime, which shut off the accretion before the disk was exhausted. There are a number of differences between the outburst pairs in the two systems; in Swift J1756.9–2508 the pairs of outbursts were separated by 2.1 and 1.2 yr,

whereas for the other systems, it was 30 d. IGR J00291+5934 has a brown dwarf donor, whereas Swift J1756.9–2508 probably has a He WD donor. Hence, the size and composition of the disk are very different in these two systems. Furthermore, IGR J00291+5934 rotates at 599 Hz, substantially faster than Swift J1756.9–2508 at 182 Hz; the other system exhibiting outburst pairs, XTE J1118+480, has a black hole primary.

While an assessment of the outburst behavior in SwiftJ 1756.9−2508 in the context of the disk instability model is beyond the scope of this paper, the accumulated outburst history of the three sources that have been observed to exhibit such double outbursts appears to offer an excellent opportunity for a more in-depth and comprehensive comparison, which may provide significant new insights into the disk instability mechanism.

Acknowledgements. We thank the anonymous referee for valuable comments. Z.L. thanks the International Space Science Institute in Bern for the hospitality. This work is supported by the National Key R&D Program of China (2016YFA0400800). Z.L. was supported by National Natural Science Foundation of China (U1938107, 11703021, U1838111, 11873041), and Scientific Research Fund of Hunan Provincial Education Department (18B059). J.P. and S.S.T. were supported by the grant 14.W03.31.0021 of the Ministry of Science and Higher Education of the Russian Federation and the Academy of Finland grants 317552, 322779, 324550, 331951, and 333112. S.Z. and S.N.Z. were supported by National Natural Science Foundation of China (Nos. U1838201 and U1838202). This research has made use of data obtained from the High Energy Astrophysics Science Archive Research Center (HEASARC), provided by NASA's Goddard Space Flight Center, and also from the HXMT mission, a projsect funded by the China National Space Administration (CNSA) and the Chinese Academy of Sciences (CAS).

References

Alpar, M. A., Cheng, A. F., Ruderman, M. A., & Shaham, J. 1982, Nature, 300, 728
Altamirano, D., Patruno, A., Heinke, C. O., et al. 2010, ApJ, 712, L58
Arnaud, K. A. 1996, in Astronomical Data Analysis Software and Systems V, eds. G. H. Jacoby, & J. Barnes, ASP Conf. Ser., 101, 17
Arzoumanian, Z., Gendreau, K. C., Baker, C. L., et al. 2014, in Space Telescopes and Instrumentation 2014: Ultraviolet to Gamma Ray, SPIE Conf. Ser., 9144, 914420
Bachetti, M., Markwardt, C. B., Grefenstette, B. W., et al. 2021, ApJ, 908, 184
Bildsten, L., & Chakrabarty, D. 2001, ApJ, 557, 292
Bozzo, E., Pjanka, P., Romano, P., et al. 2016, A&A, 589, A42
Buccheri, R., Bennett, K., Bignami, G. F., et al. 1983, A&A, 128, 245
Bult, P., Altamirano, D., Arzoumanian, Z., et al. 2018a, ApJ, 864, 14
Bult, P. M., Gendreau, K. C., Ray, P. S., et al. 2018b, ATel, 11502, 1
Bult, P. M., Gendreau, K. C., Ray, P. S., et al. 2018c, ATel, 11581, 1
Bult, P. M., Arzoumanian, Z., & Gendreau, K. C. 2020, ATel, 13760, 1
Campana, S., & Di Salvo, T. 2018, in The Physics and Astrophysics of Neutron Stars, eds. L. Rezzolla, P. Pizzochero, D. I. Jones, N. Rea, & I. Vidaña (Berlin, Heidelberg: Springer), ASSL, 457, 149
Campana, S., Ravasio, M., Israel, G. L., Mangano, V., & Belloni, T. 2003, ApJ, 594, L39
Cao, X., Jiang, W., Meng, B., et al. 2020, Sci. China Phys. Mech. Astron., 63
Chakraborty, M., & Bhattacharyya, S. 2018, ATel, 11566, 1
Chen, Y., Cui, W., Li, W., et al. 2020, Sci. China Phys. Mech. Astron., 63
Courvoisier, T. J.-L., Walter, R., Beckmann, V., et al. 2003, A&A, 411, L53
Cumming, A. 2003, ApJ, 595, 1077
De Falco, V., Kuiper, L., Bozzo, E., et al. 2017a, A&A, 603, A16
De Falco, V., Kuiper, L., Bozzo, E., et al. 2017b, A&A, 599, A88
Degenaar, N., Miller, J. M., Wijnands, R., Altamirano, D., & Fabian, A. C. 2013, ApJ, 767, L37
Deloye, C. J., & Bildsten, L. 2003, ApJ, 598, 1217
den Herder, J. W., Brinkman, A. C., Kahn, S. M., et al. 2001, A&A, 365, L7
Di Salvo, T., & Sanna, A. 2020, ArXiv e-prints [arXiv:2010.09005]
Falanga, M., Kuiper, L., Poutanen, J., et al. 2005a, A&A, 444, 15
Falanga, M., Bonnet-Bidaud, J. M., Poutanen, J., et al. 2005b, A&A, 436, 647
Falanga, M., Chenevez, J., Cumming, A., et al. 2008, A&A, 484, 43
Falanga, M., Kuiper, L., Poutanen, J., et al. 2011, A&A, 529, A68
Falanga, M., Kuiper, L., Poutanen, J., et al. 2012, A&A, 545, A26
Ferrigno, C., Bozzo, E., Falanga, M., et al. 2011, A&A, 525, A48
Frank, J., King, A., & Raine, D. J. 2002, Accretion Power in Astrophysics: Third Edition, 398
Galloway, D. K., & Cumming, A. 2006, ApJ, 652, 559
Galloway, D. K., & Keek, L. 2021, in Timing Neutron Stars: Pulsations, Oscillations and Explosions, eds. T. M. Belloni, M. Méndez, & C. Zhang (Berlin, Heidelberg: Springer), ASSL, 461, 209
Galloway, D. K., Chakrabarty, D., Morgan, E. H., & Remillard, R. A. 2002, ApJ, 576, L137
Galloway, D. K., Markwardt, C. B., Morgan, E. H., Chakrabarty, D., & Strohmayer, T. E. 2005, ApJ, 622, L45
Galloway, D. K., Muno, M. P., Hartman, J. M., Psaltis, D., & Chakrabarty, D. 2008, ApJS, 179, 360
Galloway, D. K., in't Zand, J., Chenevez, J., et al. 2020, ApJS, 249, 32
Gierliński, M., & Poutanen, J. 2005, MNRAS, 359, 1261
Goldwurm, A., David, P., Foschini, L., et al. 2003, A&A, 411, L223
Gros, A., Goldwurm, A., Cadolle-Bel, M., et al. 2003, A&A, 411, L179
Hartman, J. M., Patruno, A., Chakrabarty, D., et al. 2008, ApJ, 675, 1468
Hartman, J. M., Patruno, A., Chakrabarty, D., et al. 2009, ApJ, 702, 1673
Hartman, J. M., Galloway, D. K., & Chakrabarty, D. 2011, ApJ, 726, 26
Heger, A., Cumming, A., Galloway, D. K., & Woosley, S. E. 2007, ApJ, 671, L141
Iaria, R., Sanna, A., Di Salvo, T., et al. 2021, A&A, 646, A120
in't Zand, J. J. M., Jonker, P. G., & Markwardt, C. B. 2007, A&A, 465, 953
Kaaret, P., Morgan, E. H., Vanderspek, R., & Tomsick, J. A. 2006, ApJ, 638, 963
Keek, L., Iwakiri, W., Serino, M., et al. 2017, ApJ, 836, 111
King, A. R., & Ritter, H. 1998, MNRAS, 293, L42
Krimm, H. A., Barthelmy, S. D., Barbier, L., et al. 2007a, ATel, 1105, 1
Krimm, H. A., Markwardt, C. B., Deloye, C. J., et al. 2007b, ApJ, 668, L147
Krimm, H. A., Barthelmy, S. D., Cummings, J. R., et al. 2018, ATel, 11505, 1
Kuiper, L., Tsygankov, S., Falanga, M., Galloway, D., & Poutanen, J. 2018, ATel, 11603, 1
Kuiper, L., Tsygankov, S. S., Falanga, M., et al. 2020, A&A, 641, A37
Lebrun, F., Leray, J. P., Lavocat, P., et al. 2003, A&A, 411, L141
Lewin, W. H. G., van Paradijs, J., & Taam, R. E. 1993, Space Sci. Rev., 62, 223
Li, Z., De Falco, V., Falanga, M., et al. 2018, A&A, 620, A114
Linares, M., Wijnands, R., van der Klis, M., et al. 2008, ApJ, 677, 515
Liu, C., Zhang, Y., Li, X., et al. 2020, Sci. China Phys. Mech. Astron., 63
Lund, N., Budtz-Jørgensen, C., Westergaard, N. J., et al. 2003, A&A, 411, L231
Markwardt, C. B., Krimm, H. A., & Swank, J. H. 2007, ATel, 1108, 1
Mazzola, S., Bozzo, E., Kuulkers, E., et al. 2018, ATel, 11523, 1
Mereminskiy, I. A., Grebenev, S. A., Krivonos, R. A., & Sunyaev, R. A. 2018, ATel, 11497, 1
Nakajima, M., Sugita, S., Serino, M., et al. 2020, ATel, 13754, 1
Ng, M., Ray, P. S., Bult, P., et al. 2021, ApJ, 908, L15
Paczyński, B. 1971, ARA&A, 9, 183
Papitto, A., Riggio, A., di Salvo, T., et al. 2010, MNRAS, 407, 2575
Papitto, A., Ferrigno, C., Bozzo, E., et al. 2013, Nature, 501, 517
Papitto, A., Falanga, M., Hermsen, W., et al. 2020, New Astron. Rev., 91
Patruno, A., & Watts, A. L. 2021, in Timing Neutron Stars: Pulsations, Oscillations and Explosions, eds. T. M. Belloni, M. Méndez, & C. Zhang (Berlin, Heidelberg: Springer), ASSL, 461, 143
Patruno, A., Markwardt, C. B., Strohmayer, T. E., et al. 2009a, ATel, 2130, 1
Patruno, A., Rea, N., Altamirano, D., et al. 2009b, MNRAS, 396, L51
Patruno, A., Altamirano, D., & Messenger, C. 2010, MNRAS, 403, 1426
Poutanen, J. 2006, Adv. Space Res., 38, 2697
Poutanen, J., & Svensson, R. 1996, ApJ, 470, 249
Powell, C. R., Haswell, C. A., & Falanga, M. 2007, MNRAS, 374, 466
Rai, B., & Paul, B. C. 2019, MNRAS, 489, 5858
Sanna, A., Papitto, A., Burderi, L., et al. 2017, A&A, 598, A34
Sanna, A., Pintore, F., Riggio, A., et al. 2018a, MNRAS, 481, 1658
Sanna, A., Bahramian, A., Bozzo, E., et al. 2018b, A&A, 610, L2
Sanna, A., Ferrigno, C., Ray, P. S., et al. 2018c, A&A, 617, L8
Sanna, A., Pintore, F., Riggio, A., et al. 2019, ATel, 12882, 1
Strohmayer, T., & Bildsten, L. 2006, in Compact Stellar X-ray Sources, eds. W. Lewin, & M. van der Klis (Cambridge: Cambridge University Press), Cambridge Astrophys. Ser., 39, 113
Strohmayer, T. E., Arzoumanian, Z., Bogdanov, S., et al. 2018, ApJ, 858, L13
Strüder, L., Briel, U., Dennerl, K., et al. 2001, A&A, 365, L18
Turner, M. J. L., Abbey, A., Arnaud, M., et al. 2001, A&A, 365, L27
Ubertini, P., Lebrun, F., Di Cocco, G., et al. 2003, A&A, 411, L131
Wijnands, R. in Trends in Pulsar Research, ed. J. A. Lowry, 53, 2006
Wijnands, R., & van der Klis, M. 1998, Nature, 394, 344
Winkler, C., Courvoisier, T. J.-L., Di Cocco, G., et al. 2003, A&A, 411, L1
Zhang, S.-N., Li, T., Lu, F., et al. 2020, Sci. China Phys. Mech. Astron., 63